

Article

Application of Fe-Impregnated Biochar from Cattle Manure for Removing Pentavalent Antimony from Aqueous Solution

Seong-Jik Park ^{1,*}, Yeon-Jin Lee ¹, Jin-Kyu Kang ², Je-Chan Lee ³ and Chang-Gu Lee ³

¹ Department of Bioresources and Rural Systems Engineering, Hankyong National University, Anseong 17579, Korea; 2018125014@hknu.ac.kr

² Research Institute of Agriculture and Life Sciences, Seoul National University, Seoul 08826, Korea; naengie@snu.ac.kr

³ Department of Environmental and Safety Engineering, Ajou University, Suwon 16499, Korea; jlee83@ajou.ac.kr (J.-C.L.); changgu@ajou.ac.kr (C.-G.L.)

* Correspondence: parkseongjik@hknu.ac.kr; Tel.: +82-31-670-5131

Abstract: This study assessed the applicability of Fe-impregnated biochar derived from cattle manure (Fe-CMB) as an adsorbent for removing Sb(V) from aqueous solutions and investigated the Sb(V) adsorption mechanism. Fe-CMB was mainly composed of C, O, Cl, Fe, Ca, and P, and the adsorption of Sb(V) onto Fe-CMB was identified using an energy dispersive spectrometer and Fourier transform infrared spectroscopy. Sb(V) adsorption reached equilibrium within 6 h, and the Sb(V) adsorption data as a function of time were well described by the pseudo-second-order model. The Langmuir isotherm model fit the equilibrium data better than the Freundlich model. The maximum adsorption capacity of Fe-CMB for Sb(V) obtained from the Langmuir model was 58.3 mg/g. Thermodynamic analysis of Sb(V) adsorption by Fe-CMB indicated that the adsorption process was exothermic and spontaneous. The Sb(V) removal percentage increased with the Fe-CMB dose, which achieved a removal of 98.5% at 10.0 g/L Fe-CMB. Increasing the solution pH from 3 to 11 slightly reduced Sb(V) adsorption by 6.5%. The inhibitory effect of anions on Sb(V) adsorption followed the order: $\text{Cl}^- \approx \text{NO}_3^- < \text{SO}_4^{2-} < \text{HCO}_3^- < \text{PO}_4^{3-}$.

Keywords: antimony; biochar; cattle manure; removal; adsorption; Fe impregnation



Citation: Park, S.-J.; Lee, Y.-J.; Kang, J.-K.; Lee, J.-C.; Lee, C.-G. Application of Fe-Impregnated Biochar from Cattle Manure for Removing Pentavalent Antimony from Aqueous Solution. *Appl. Sci.* **2021**, *11*, 9257. <https://doi.org/10.3390/app11199257>

Academic Editors: Angeles Sanroman Braga and Emilio Rosales Villanueva

Received: 1 September 2021

Accepted: 4 October 2021

Published: 5 October 2021

Publisher's Note: MDPI stays neutral with regard to jurisdictional claims in published maps and institutional affiliations.



Copyright: © 2021 by the authors. Licensee MDPI, Basel, Switzerland. This article is an open access article distributed under the terms and conditions of the Creative Commons Attribution (CC BY) license (<https://creativecommons.org/licenses/by/4.0/>).

1. Introduction

Antimony (Sb), a hazardous element that is toxic to human health, causes several diseases such as respiratory irritation, pneumoconiosis, high blood cholesterol, low blood sugar, and cancer [1,2]. Due to the high toxicity and hazardousness of Sb, the World Health Organization (WHO) and some countries regulate its standard concentration in drinking water: WHO, 20.0 µg/L [3]; the United States Environmental Protection Agency, 6.0 µg/L [4]; and European Union, 5.0 µg/L [5]. The Korean government does not provide guidelines to regulate Sb concentration in drinking water, but its concentration in wastewater is controlled to below 0.02 mg/L. Sb is predominant in nature as Sb(OH)₃ and Sb(OH)₆[−], and Sb(III) and Sb(V) are usually present in reducing and oxidizing water environments, respectively [6]. The stability and solubility of Sb(V) is higher than that of Sb(III), which prevails in water bodies by mostly remaining in an oxidizing environment [7]. Therefore, more efforts are needed to develop efficient technologies to remove Sb(V) from aqueous solutions.

Because of the toxicity of Sb, various studies including coagulation, membrane separation, electrodeposition, bioremediation, and adsorption have been performed to remove Sb from aqueous solutions [8]. Among them, adsorption has been considered sustainable and efficient for Sb removal because of its high efficiency, cost-effectiveness, and simple operation [9]. The efficiency and cost of the adsorption process depend highly on the

selection of adsorbents, and various adsorbents have been explored in removing target contaminants under different environmental conditions.

Because of its porous structure, large specific surface area, abundant functional groups on the surface, and high stability, application of biochar in environmental remediation has attracted the interest of many researchers [10]. A wide range of organic materials, such as agricultural byproducts, sawdust, animal manure, and sludge, can be used as raw materials to produce biochar [11]. Biochar has been extensively applied to adsorb heavy metals such as Cd, Cu, Cr, and Zn [12]. Biochar has attracted the attention of many researchers as an adsorbent alternative to activated carbon, which has been most widely used but is costly [13]. The efficiency of heavy metal removal by biochar is influenced by the physicochemical properties of biochar, biochar dosage, pH, water temperature, and initial concentrations and types of heavy metals [14]. However, research on biochar-mediated Sb removal has only been attempted recently [1,8–10,15,16].

Nascent biochar is relatively ineffective in removing anions and oxyanions such as fluoride, phosphate, Se, As, and Cr; hence, modifying the biochar to enhance its anion adsorption capacity has been explored. Fe impregnation has been an inexpensive and highly effective method in enhancing the biochar adsorption capacity for As removal [17]. Since Sb and As belong to group 15 in the periodic table, Sb exhibits many similar chemical characteristics and behaviors as As in natural water [8]. In addition, Fe oxides and hydroxides have been reported to strongly bind to Sb(III) and Sb(V) [18].

In our previous study [19], cattle manure pyrolyzed in the presence of Fe produced valuable energy fuels (gas and oil) and biochar, which effectively removed selenate. Animal manure has been applied to cropland as an organic fertilizer for replenishing the N, P, Ca, and K, but their excessive application has resulted in environmental and public health issues such as water pollution and the occurrence of pathogen, odors, and bugs [20,21]. Therefore, more efficient, inexpensive, and environmentally sustainable methods for treating them have been explored, and thermal-chemical processes including anaerobic digestion, combustion, gasification, and pyrolysis have been considered a promising technology to treat animal manure and produce biomass energies [20]. Pyrolysis and gasification are the most widely used thermo-chemical treatments for cattle manures; in pyrolysis, carbonaceous materials are thermally decomposed into biochar, liquid biofuels, and gaseous fuel at relatively low temperature (450–600 °C) without oxygen. Gasification produces syngas by adding gasifying agents such as air, steam, and air-steam [22]. Pyrolysis results in a much higher biochar yield (~50 wt.%) than gasification (~10 wt.%) [23].

In this study, Fe-impregnated biochar derived from cattle manure (Fe-CMB) was used for the removal of Sb(V) from an aqueous solution. The physical and chemical properties of the Fe-CMB before and after Sb(V) adsorption were analyzed, and the Sb(V) adsorption by Fe-CMB was characterized under various experimental conditions including kinetics, equilibrium, thermodynamics, adsorbent dosage, pH, and the presence of anions.

2. Materials and Methods

2.1. Preparation and Characterization of Fe-CMB

The procedure to synthesize Fe-CMB is described in our previous study [19]. Cattle manure obtained from a local dairy farm was dried at 70 °C for 24 h before producing biochar. Dried cattle manure (200 g) was soaked in 1 L of 6% FeCl₃ solution for 30 min. This mixture of cattle manure and FeCl₃ was agitated for 2 h and dried at 70 °C for 24 h. Cattle manure was pyrolyzed at 500 °C in a quartz tubular furnace (HTF-Q60, Hantech, Korea) for 3.5 h. Anoxic conditions were produced by injecting N₂ gas into the reactor at a flow rate of 100 mL/min.

The physical and chemical properties of Fe-CMB before and after Sb(V) adsorption were analyzed using field emission scanning electron microscopy (FE-SEM), energy-dispersive X-ray spectroscopy (EDS), and Fourier transform infrared (FT-IR) spectroscopy. The surface morphologies of the Fe-CMB were investigated using FE-SEM (S-4700, Hitachi, Tokyo, Japan) and its elemental composition was analyzed using an EDS (Genesis

XM2, EDAX, Mahwah, NJ, USA) attached to the FE-SEM. The chemical functional groups present on the surface of Fe-CMB were identified using an FT-IR spectrometer (Nicolet iS10, Thermo Scientific, Waltham, MA, USA), wherein the sample to be analyzed was prepared as a potassium bromide (KBr) pellet.

2.2. Batch Adsorption Experiments

The adsorption characteristics of Sb(V) onto Fe-CMB were investigated by performing kinetic, equilibrium, and thermodynamic experiments under batch conditions and fitting mathematical models to obtain experimental data. The performance of Fe-CMB for Sb(V) removal was also quantified under different environmental conditions by varying the Fe-CMB dose, solution pH, and adding various anions. KSb(OH)_6 (Sigma-Aldrich, Saint Louis, MO, USA) was dissolved in deionized water to prepare a stock solution of 200 mg/L, and the Sb(V) solution required for batch experiments was diluted from the stock. All batch experiments were performed using the following conditions, unless otherwise stated; Fe-CMB (0.1 g) was added into 30 mL of 50 mg-Sb/L solution in a 50 mL falcon tube and agitated using a shaking incubator (SJ-808SF, Sejong Scientific Co., Buchon, Korea), which was maintained at a constant speed of 100 rpm and a temperature of 25 °C. Kinetic experiments were performed by varying the reaction time from 0.25 h to 24 h, and equilibrium experiments were conducted under different initial concentrations in the range of 5–170 mg/L. Thermodynamic experiments were performed at different reaction temperatures set at 15, 25, and 35 °C for 24 h reaction. The Fe-CMB removal efficiency and the amount of Sb(V) adsorbed onto unit mass of Fe-CMB were quantified by varying the Fe-CMB dose amount from 3.33 g/L to 16.67 g/L. The adsorbent dose was increased until there was no increase in the removal percentage. Sb(V) adsorption by Fe-CMB was evaluated under different initial pH values of 3–11. The pH of the solution was adjusted using 1 M NaOH and 1 M HCl, and the pH was measured using a pH meter (Seven-multi S40, Mettler Toledo, Switzerland). The effect of anions on Sb adsorption was investigated using 50 mg/L of Sb solution, which was treated with 1 and 10 mM NaCl, Na_2SO_4 , NaNO_3 , NaHCO_3 , and Na_2HPO_4 .

2.3. Adsorption Modeling

The kinetic data were analyzed using pseudo-first-order (Equation (1)), pseudo-second-order (Equation (2)), and pseudo-nth-order (Equation (3)) models, and the equations are as follows [24]:

$$q_t = q_e \left(1 - e^{-k_1 t}\right) \quad (1)$$

$$q_t = \frac{k_2 q_e^2 t}{1 + k_2 q_e t} \quad (2)$$

$$q_t = q_e \left\{ 1 - \frac{1}{\left[1 + (n-1)q_e^{n-1} k_n t\right]^{1/(n-1)}} \right\} \quad (3)$$

where q_t is the adsorbed amount of Sb(V) onto Fe-CMB at time t (mg/L), q_e is the adsorbed amount of Sb(V) onto Fe-CMB at equilibrium, k_1 is the rate constant of pseudo-first-order model (1/h), k_2 is the rate constant of pseudo-second-order model (g/mg/h), k_n is the rate constant of pseudo-nth-order model ($\text{g}^{n-1}/\text{mg}^{n-1}/\text{h}$), and n is the reaction order of pseudo-nth-order model.

Langmuir (Equation (4)), Freundlich (Equation (5)), and Temkin (Equation (6)) models were employed to analyze the equilibrium data, and the equations are as follows [25]:

$$q_e = \frac{Q_m K_L C_e}{1 + K_L C_e} \quad (4)$$

$$q_e = K_F C_e^{\frac{1}{n}} \quad (5)$$

$$q_e = \frac{RT}{B_T} \ln(K_T C_e) \quad (6)$$

where C_e is the Sb(V) concentration in the aqueous solution at equilibrium (mg/L), K_L is the Langmuir constant related to the binding energy (L/mg), Q_m is the monolayer saturation capacity at a given condition, which indicates the maximum Sb(V) adsorption capacity of Fe-CMB (mg/g), K_F is the distribution coefficient ((mg/g)·(L/mg)^{1/n}), and n is the Freundlich constant. K_T is the Temkin constant (L/g), B_T is related to the heat of sorption (kJ/mol), and R is the gas constant (8.314 J/mol·K).

The values of K_L , Q_m , K_F , n , K_T , and B_T were determined by fitting the experimental data to the Langmuir, Freundlich, and D-R models. All model parameters were obtained by non-linear regression with the highest determination coefficient (R^2) and lowest sum of squared error (SSE) using Microsoft Excel 2016.

The thermodynamic properties of Sb(V) adsorption by Fe-CMB were calculated using the following equation:

$$\Delta G^0 = \Delta H^0 - T\Delta S^0 \quad (7)$$

$$\Delta G^0 = -RT \ln K_e \quad (8)$$

$$\ln K_e = \frac{\Delta S^0}{R} - \frac{\Delta H^0}{RT} \quad (9)$$

$$K_e = \frac{\alpha q_e}{C_e} \quad (10)$$

where ΔG^0 is the change in Gibbs free energy (kJ/mol), ΔS^0 is the change in entropy (J/mol/K), ΔH^0 is the change in enthalpy (kJ/mol), R is the gas constant (J/mol/K), K_e is the equilibrium constant (-), T is the absolute temperature (K), and α is the amount of adsorbent (g/L).

3. Results and Discussion

3.1. Physical and Chemical Characteristics of Fe-CMB

Figure 1 shows the surface morphologies of Fe-CMB obtained from FE-SEM, revealing a rough and porous surface with round lumps. Interestingly, the porous structure of Fe-CMB was maintained despite Sb(V) adsorption. Furthermore, Fe-CMB is mainly composed of C, O, Cl, Fe, and Ca (Table 1). After the adsorption experiments, the Cl and Ca contents of Fe-CMB reduced significantly, indicating their loss during adsorption. The Fe on the surface of Fe-CMB did not decrease and detach despite the adsorption experiments, indicating that Fe was firmly bound to the biochar surface.

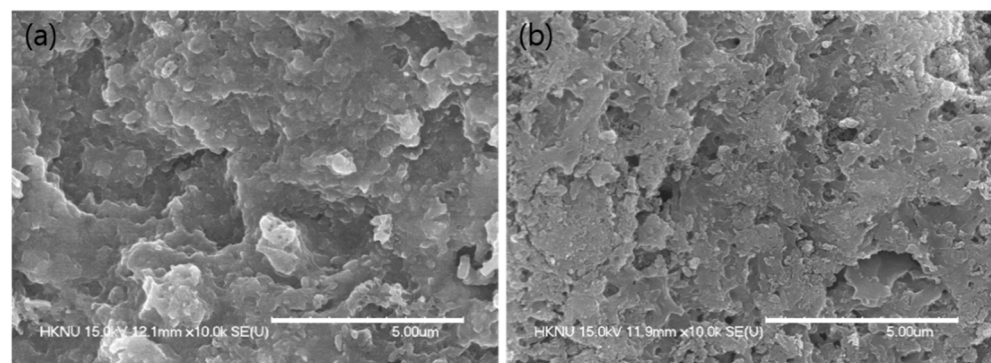
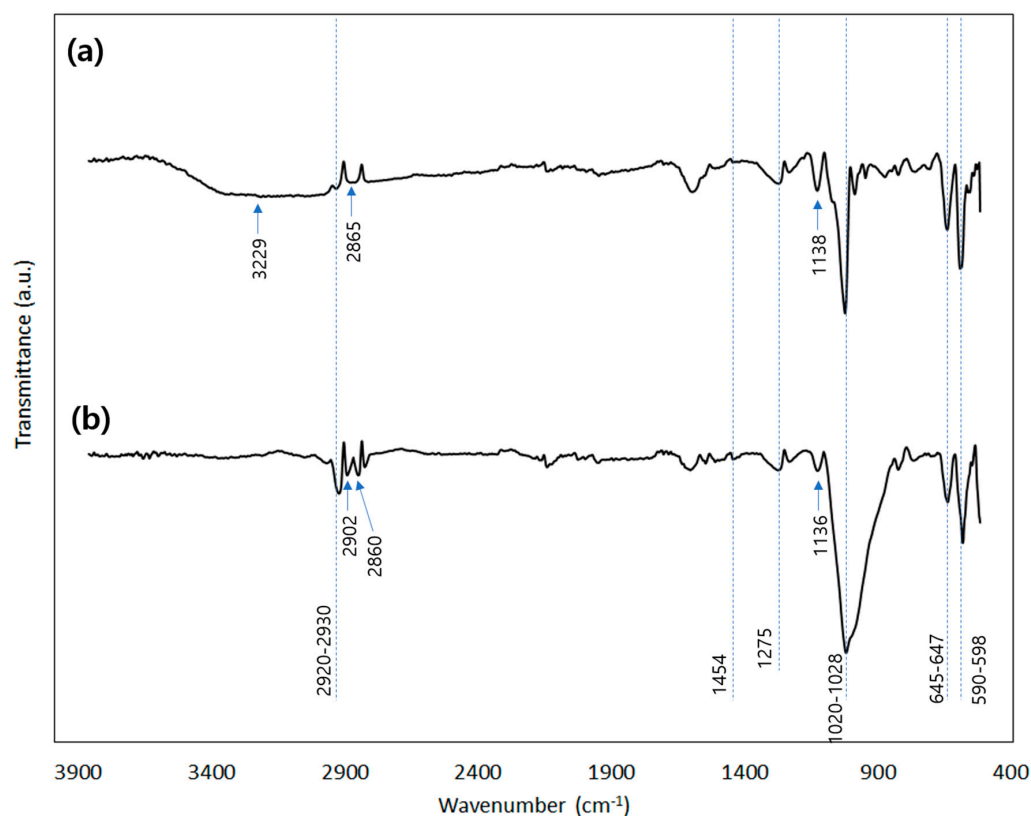


Figure 1. Surface morphologies of Fe-CMB (a) before and (b) after Sb(V) adsorption. Analyzed using a field emission scanning electron microscope.

Table 1. Elemental composition (weight %) of Fe-CMB obtained from energy dispersive spectrometer.

| Fe-CMB | C | O | Cl | Fe | Ca | P | Mg | K | S | Si |
|--------------------|------------|------------|------------|------------|------------|-----------|-----------|-----------|-----------|-----------|
| Before ad-sorption | 28.0 ± 1.4 | 15.8 ± 2.1 | 18.0 ± 4.4 | 14.6 ± 0.8 | 10.2 ± 1.5 | 6.2 ± 1.8 | 2.2 ± 0.2 | 2.1 ± 0.1 | 1.9 ± 1.5 | 1.3 ± 0.4 |
| After ad-sorption | 30.4 ± 1.3 | 19.7 ± 3.1 | 1.8 ± 0.4 | 31.9 ± 3.6 | 0.0 ± 0.0 | 8.4 ± 4.2 | 0.4 ± 0.0 | 0.3 ± 0.0 | 4.2 ± 3.9 | 0.3 ± 0.0 |

Fe-CMB and Sb(V)-adsorbed Fe-CMB displayed several distinctive peaks, as shown in Figure 2. The broad band at 3229 cm^{-1} corresponds to the O-H bending vibration [10]. The peaks observed at $2920\text{--}2930$ and $2860\text{--}2865\text{ cm}^{-1}$ correspond to the methylene C-H asymmetric/symmetric stretch, while the peak at 1454 cm^{-1} also corresponds to the methylene C-H bend [26]. The peaks at approximately 1135 and $1020\text{--}1028\text{ cm}^{-1}$ represent the skeletal C-C vibrations [26]. The peaks near 600 cm^{-1} are attributed to O-H out-of-plane bending [26]. The peaks observed between 650 and 1275 cm^{-1} are ascribed to $\equiv\text{Fe-O}$ [27]. The changes in the peaks after Sb(V) adsorption differ from those in previous studies, where Sb(V) was removed using metal oxides. McComb et al. [28] reported that the intensity of the peaks at approximately 1100 and 3200 cm^{-1} increased while Sb(V) was adsorbed onto iron oxide by inner-sphere complex with the contribution of hydroxyl groups from adsorbed antimonate. Although the results of this study were dissimilar to those of a previous study [28], peak improvement at 1020 cm^{-1} evidently indicated the adsorption of Sb(V). The peak at 1020 cm^{-1} is generated by the $\delta(\text{OH})$ of hexahydroxyantimonate salt, which may probably be enhanced by the adsorption of Sb(V) [27]. This suggests that Sb(V) is adsorbed onto Fe-CMB via electrostatic attraction or ion exchange.

**Figure 2.** Fourier transform infrared spectroscopy spectra of Fe-CMB (a) before and (b) after Sb(V) adsorption.

3.2. Kinetic Adsorption Experiments

Sb(V) adsorption as a function of reaction time with model fit is presented in Figure 3, and the model parameters obtained by kinetic models using experimental data are given in

Table 2. Sb(V) adsorption increased sharply within 1 h and continued to gradually increase until 6 h. A high adsorption rate was observed at the beginning of the reaction because of the availability of favorable adsorption sites, which then decreased near the equilibrium time owing to the saturation of favorable adsorption sites [29].

The pseudo-second-order model had a higher R^2 and lower SSE than that of the pseudo-first-order model. The q_e obtained from the pseudo-second-order model is closer to the experimentally obtained q_e , 13.1 mg/g. These results indicate that the pseudo-second-order model describes the kinetic adsorption of Fe-CMB-mediated Sb(V) better than the pseudo-first-order model. The order of kinetic reactions, identified from n values of the pseudo- n th-order model, were approximately 2, which is consistent with the suitability of the pseudo-second-order model. A better description of the experimental data by the pseudo-second-order model than the pseudo-first-order model indicates that the rate of Sb(V) adsorption by Fe-CMB is mainly controlled by chemical adsorption [30].

Table 2. Model parameters and model suitability for kinetic adsorption data obtained from pseudo-first-order, pseudo-second-order, and pseudo- n th-order models.

| | Model Parameter | | | R^2 | SSE |
|----------------------|----------------------|-------------------------------------|---------------------------|-------|-------|
| Pseudo-first-order | q_e (mg/g) 12.7 | | k_1 (1/min) 5.512 | 0.896 | 2.494 |
| Pseudo-second-order | q_e (mg/g) 13.1 | | k_2 (g/mg/min) 0.919 | 0.977 | 0.562 |
| Pseudo- n th-order | q_e (mg/g) 13.3 | k_n ((mg/g) $^{1-n}$ /h) 0.592 | n 2.245 | 0.978 | 0.527 |

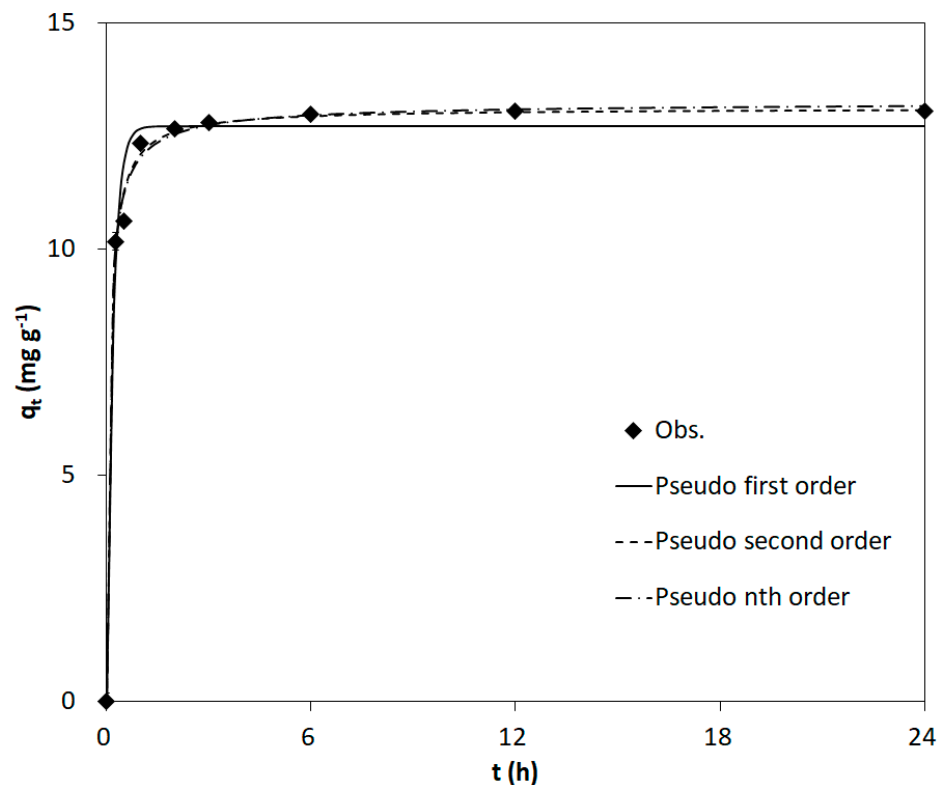


Figure 3. Kinetic adsorption results of Sb(V) adsorption by Fe-CMB and model fits using pseudo-first-order, pseudo-second-order, and pseudo- n th-order models.

3.3. Equilibrium Adsorption Experiments

The Sb(V) concentrations in the aqueous and solid phases at equilibrium are plotted in Figure 4, and the parameters of the equilibrium adsorption models are provided in Table 3. The adsorption amount increased with increasing initial concentrations, and Sb(V)

adsorbed onto Fe-CMB reached a plateau at an initial concentration of 150 mg/L. The driving force for Sb(V) adsorption was minimal at low initial concentrations owing to small Sb(V) concentration gradient between the aqueous and solid phases [29].

A higher R^2 and lower SSE values of the Langmuir model than those of the Freundlich model indicate that Sb(V) is adsorbed by Fe-CMB through monolayer adsorption rather than multilayer adsorption. The Temkin model, derived using molecular statistical theory [25], fit the least with $R^2 = 0.877$. The heat of Sb(V) adsorption calculated from the Temkin model was 0.217 kJ/mol. The $1/n$ value of the Freundlich model was 0.575, which is slightly higher than 0.5, indicating that the intensity of Sb(V) adsorption is slightly weak [31]. The maximum adsorption capacity of Fe-CMB obtained from the Langmuir model was 58.3 mg/g, which was higher than that of the other adsorbents such as Ce-doped magnetic biochar: 25.0 mg/g [9]; α -Fe₂O₃: 11.0 mg/g [32]; manganese iron oxide: 10.0 mg/g [33]; goethite nanopowder: 7.5 mg/g [34], as reported in literatures. This result indicates that Fe-CMB can be used as a promising adsorbent for Sb(V) removal from aqueous solutions.

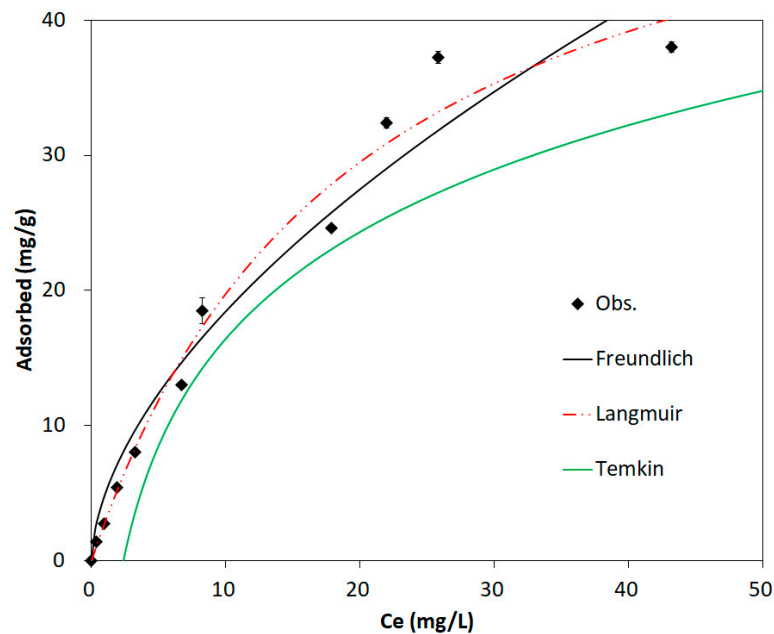


Figure 4. Equilibrium adsorption results for Sb(V) adsorption by Fe-CMB and model fits using Freundlich, Langmuir, and Temkin models.

Table 3. Model parameters and model suitability for equilibrium adsorption data obtained from Freundlich, Langmuir, and Temkin models.

| | Model Parameter | | R^2 | SSE |
|------------|-----------------|--------------|-------|-------|
| Freundlich | K_F (L/g) | $1/n$ (-) | 0.960 | 83.8 |
| | 4.910 | 0.575 | | |
| Langmuir | Q_m (mg/g) | K_L (L/mg) | 0.982 | 39.1 |
| | 58.3 | 0.051 | | |
| Temkin | B_T (kJ/mol) | K_T (L/g) | 0.877 | 260.3 |
| | 0.217 | 0.423 | | |

3.4. Thermodynamic Adsorption Experiments

The Van't Hoff plot obtained from Sb(V) adsorption experiments at 15, 25, and 35 °C are presented in Figure 5, and the enthalpy (ΔH^0), entropy (ΔS^0), and Gibbs free energy (ΔG^0) obtained from the thermodynamic analysis are presented in Table 4. The Sb(V) adsorption by Fe-CMB decreased with increasing reaction temperature, which is consistent with the negative value of ΔH^0 . The negative value of ΔH^0 indicates that Sb(V) adsorption

onto Fe-CMB is exothermic. The free energy (ΔG^0) values under all conditions in this study were negative, which suggests that the Sb(V) adsorption process was spontaneous.

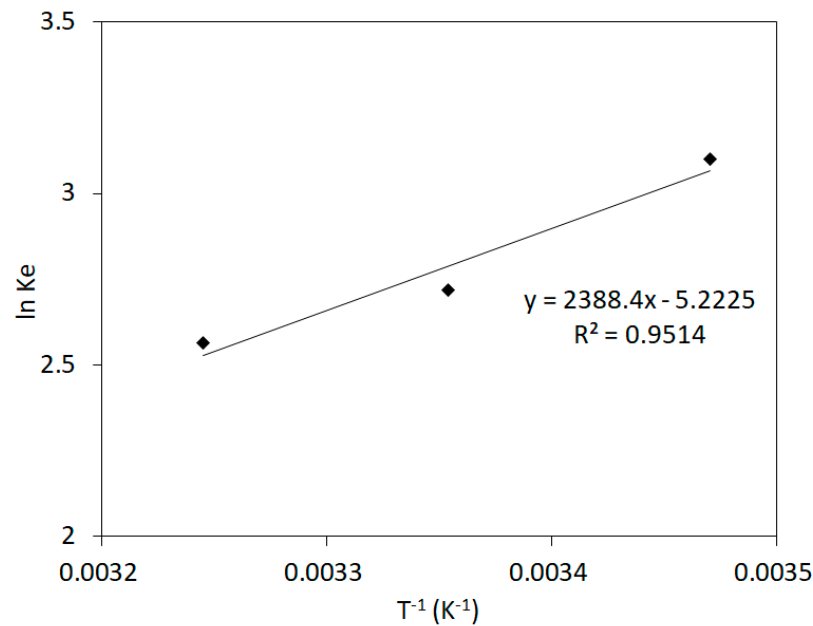


Figure 5. Van't Hoff plot for Sb(V) adsorption by Fe-CMB.

Table 4. Enthalpy, entropy, and Gibb's free energy for the adsorption of Sb(V) by Fe-CMB.

| Temp. (°C) | $\ln K_e$ | $1/T (1/K)$ | $\Delta H^0 (kJ/mol)$ | $\Delta S^0 (J/K \cdot mol)$ | $\Delta G^0 (kJ/mol)$ | R^2 |
|------------|-----------|-------------|-----------------------|------------------------------|-----------------------|--------|
| 15 | 3.099984 | 0.003470 | | | −7.35 | |
| 25 | 2.71791 | 0.003354 | −19.86 | −43.42 | −6.91 | 0.9514 |
| 35 | 2.56438 | 0.003245 | | | −6.48 | |

3.5. Effect of Adsorbent Dosage

The amount of Sb(V) adsorbed amounts per unit mass of adsorbents and the removal percentage under different amounts of Fe-CMB are presented in Figure 6. With an increase in the Fe-CMB dose from 3.3 g/L to 16.7 g/L, the amount of Sb(V) adsorbed per unit mass of Fe-CMB decreased from 13.8 mg/g to 3.0 g/L, because the adsorption sites present on the adsorbent surface were not fully occupied by adsorbate [19]. However, at higher Fe-CMB doses, the removal percentage of Sb(V) increased because the increase of adsorbent dosage provided more available sites for Sb(V) adsorption, thereby leaving less residual concentration of Sb(V) in the aqueous phase [35]. Approximately 98.5% of Sb(V) could be removed by Fe-CMB at a dose of 10.0 g/L.

3.6. Effect of Solution pH

The Sb(V) adsorption by Fe-CMB as a function of the solution pH (3–11) is presented in Figure 7. The increase in solution pH reduced the Sb(V) adsorption from 14.2 mg/g to 13.3 mg/g. The solution pH profoundly affects adsorption by influencing the surface charge of the adsorbent and the metal species [9]. Sb(V) mainly exists as $Sb(OH)_6^-$ in the solution with pH 2–10 [10], and Sb(V) favors a positively charged surface. The surface of the adsorbent becomes more negatively charged with increasing solution pH, causing repulsion between $Sb(OH)_6^-$ and more negatively charged surfaces [9,10]. Furthermore, competing with OH^- at higher solution pH also inhibits the Sb(V) adsorption. The Sb(V) adsorption is generally higher under acidic conditions and relatively insensitive to solution pH. Although the solution pH increased from 3 to 11, the Sb(V) adsorption decreased by

only 6.5%. Fe-CMB maintained its performance at a high pH, indicating that Fe-CMB can be applied to alkaline wastewater.

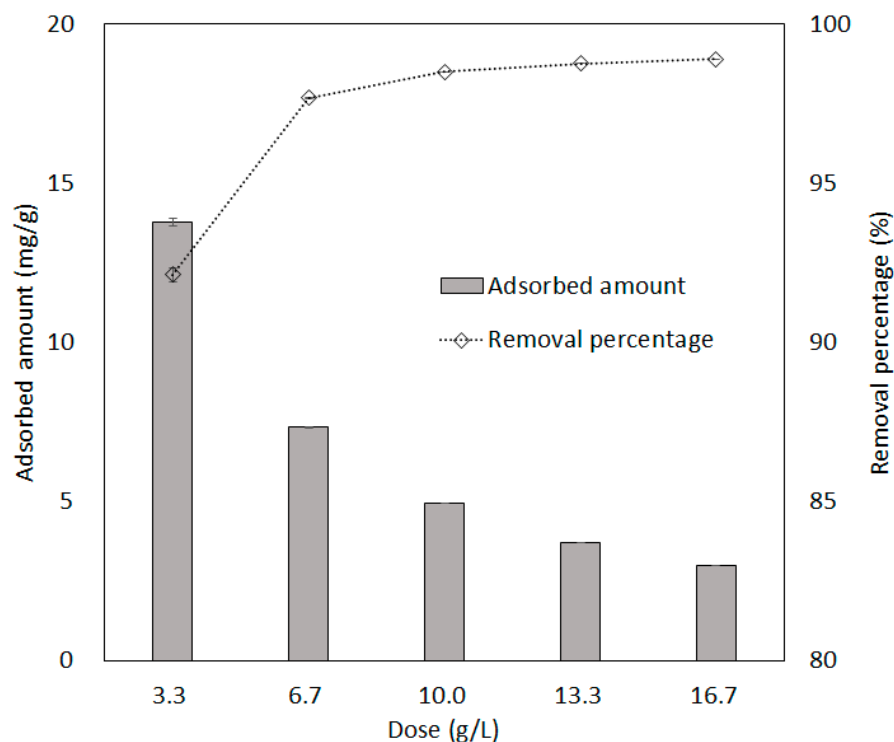


Figure 6. Effect of Fe-CMB dose on the adsorbed amount of Sb(V) per unit mass of adsorbent (mg/g) and their corresponding removal percentage (%).

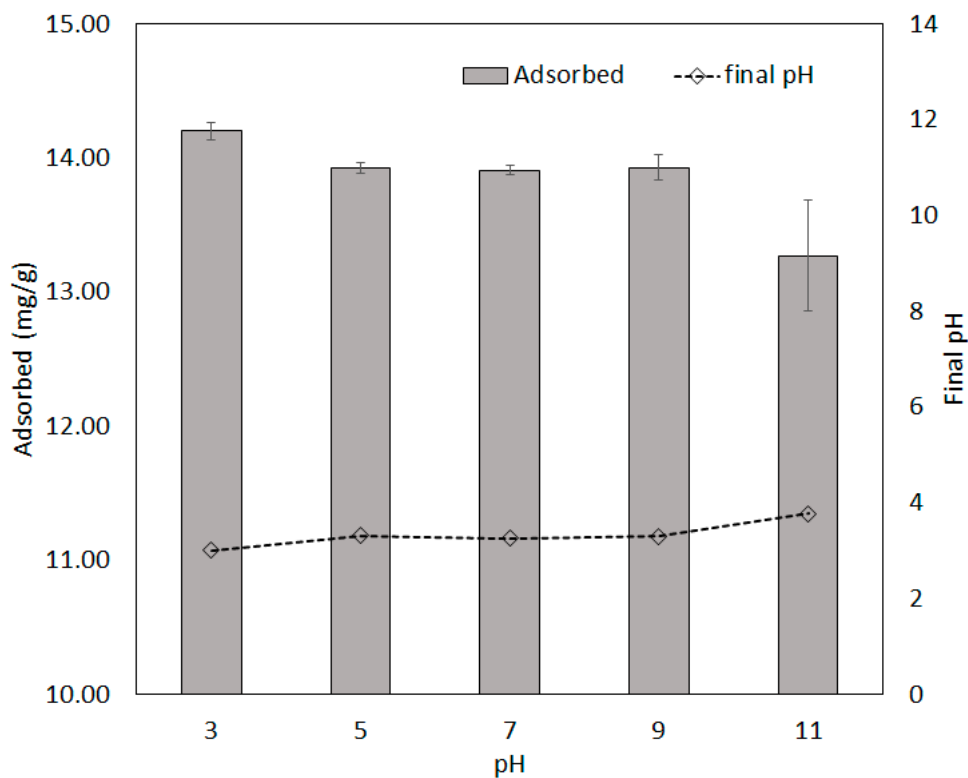


Figure 7. Adsorbed amounts of Sb(V) and final pH as a function of initial solution pH.

3.7. Effect of the Presence of Anions

Several anions such as chloride (Cl^-), sulfate (SO_4^{2-}), nitrate (NO_3^-), bicarbonate (HCO_3^-), and phosphate (PO_4^{3-}) often exist in natural water and wastewater, and they can negatively influence Sb(V) adsorption [9]. The influence of these anions on Sb(V) adsorption was investigated at two different molar concentrations, 1 and 10 mM, as shown in Figure 8. The reason for setting the anion concentration to 1 mM and 10 mM was to simulate natural water and wastewater, respectively [36]. The presence of Cl^- and NO_3^- negligibly inhibited Sb(V) adsorption because compared to Sb(V), these ions bind less strongly to the adsorbents [9]. However, HCO_3^- and PO_4^{3-} exhibited negative effects on Sb(V) adsorption, with reductions of 41.6% and 90.6% in the presence of 10 mM HCO_3^- and PO_4^{3-} , respectively. The reduction of Sb(V) adsorption onto iron-based materials by competing anions, especially PO_4^{3-} , has also been reported in other studies [2,37]. This phenomenon can be explained by the high affinity of PO_4^{3-} to iron via the formation of inner-sphere complexes [38].

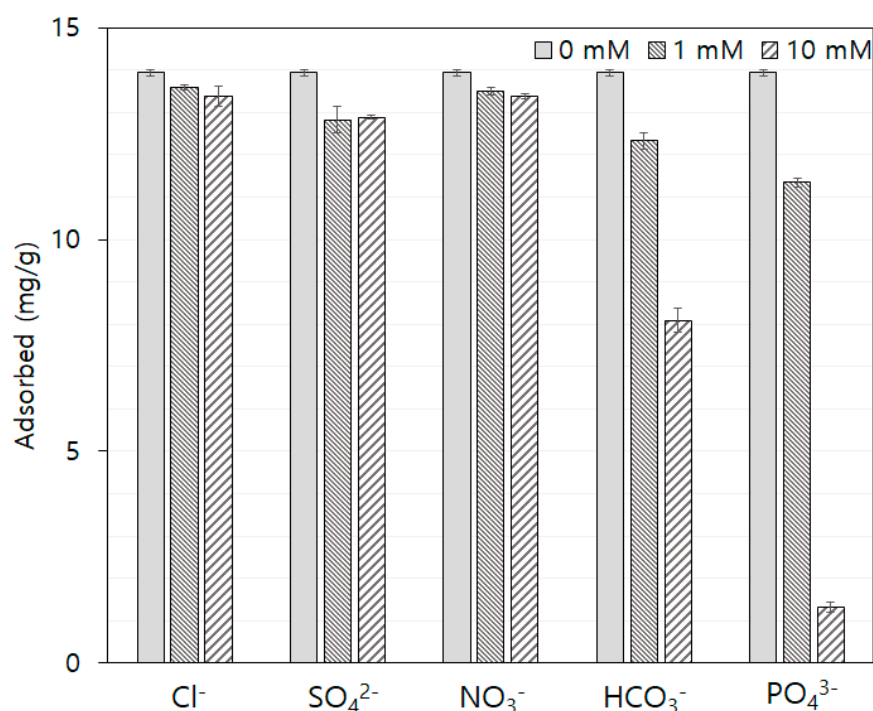


Figure 8. Sb(V) adsorption by Fe-CMB in the presence of 1 and 10 mM chloride (Cl^-), sulfate (SO_4^{2-}), nitrate (NO_3^-), bicarbonate (HCO_3^-), and phosphate (PO_4^{3-}).

4. Conclusions

Fe-CMB produced from the pyrolysis of cattle manure for generating biochar was used as an adsorbent to remove Sb(V) from aqueous solution. The adsorption kinetics and model analysis indicated that the rate of Sb(V) adsorbed was mainly controlled by chemical adsorption. The Langmuir model fit the data better than the Freundlich model, indicating that Sb(V) was adsorbed onto Fe-CMB via a monolayer. The maximum adsorption capacity of Fe-CMB for Sb(V) was 58.3 mg/g, which is higher than that of the other adsorbents reported in the literature. In this study, the adsorption of Sb(V) onto Fe-CMB was exothermic and spontaneous. Increase in initial solution pH decreased Sb(V) adsorption because of the less positive surface charge of adsorbents and competition with hydroxyl ions. However, the decrease in Sb(V) adsorption with increasing pH was unremarkable because of the low final pH observed, even for high initial pH conditions. The presence of PO_4^{3-} significantly inhibited Sb(V) adsorption due to the strong affinity of PO_4^{3-} towards Fe present on the surface of Fe-CMB. Hence, Fe-CMB can effectively remove Sb(V) even under alkaline conditions, and it can also be a potential adsorbent for other oxyanions in aqueous solutions.

Author Contributions: S.-J.P.: conceptualization, writing—original draft preparation, writing—review and editing, supervision; Y.-J.L.: methodology; J.-K.K.: validation, data curation, visualization; J.-C.L.: methodology; C.-G.L.: writing—review and editing. All authors have read and agreed to the published version of the manuscript.

Funding: This research received no external funding.

Institutional Review Board Statement: Not applicable.

Informed Consent Statement: Not applicable.

Data Availability Statement: The data presented in this study are available upon request from the corresponding author.

Conflicts of Interest: The authors declare no conflict of interest.

References

1. Vithanage, M.; Rajapaksha, A.U.; Ahmad, M.; Uchimiya, M.; Dou, X.; Alessi, D.S.; Ok, Y.S. Mechanisms of antimony adsorption onto soybean stover-derived biochar in aqueous solutions. *J. Environ. Manag.* **2015**, *151*, 443–449. [CrossRef]
2. Zhu, G.; Lin, J.; Yuan, Q.; Wang, X.; Zhao, Z.; Hursthouse, A.S.; Wang, Z.; Li, Q. A biochar supported magnetic metal organic framework for the removal of trivalent antimony. *Chemosphere* **2021**, *282*, 131068. [CrossRef] [PubMed]
3. WHO. Guidelines for Drinking-Water Quality. 2011, Volume 38, pp. 104–108. Available online: <https://www.who.int/publications/i/item/9789241549950> (accessed on 4 October 2021).
4. EPA, U.S. Edition of the Drinking Water Standards and Health Advisories. 2018. Available online: <https://www.epa.gov/sites/default/files/2018-03/documents/dwtable2018.pdf> (accessed on 4 October 2021).
5. Asher, B.; Eddo, H. Drinking Water Quality Standards and Regulations. 2012. Available online: <https://publications.jrc.ec.europa.eu/repository/handle/JRC61360> (accessed on 4 October 2021).
6. Filella, M.; Belzile, N.; Chen, Y.-W. Antimony in the environment: A review focused on natural waters: I. Occurrence. *Earth-Sci. Rev.* **2002**, *57*, 125–176. [CrossRef]
7. Li, J.; Zheng, B.; He, Y.; Zhou, Y.; Chen, X.; Ruan, S.; Yang, Y.; Dai, C.; Tang, L. Antimony contamination, consequences and removal techniques: A review. *Ecotoxicol. Environ. Saf.* **2018**, *156*, 125–134. [CrossRef]
8. Wei, D.; Li, B.; Luo, L.; Zheng, Y.; Huang, L.; Zhang, J.; Yang, Y.; Huang, H. Simultaneous adsorption and oxidation of antimonite onto nano zero-valent iron sludge-based biochar: Indispensable role of reactive oxygen species and redox-active moieties. *J. Hazard. Mater.* **2020**, *391*, 122057. [CrossRef] [PubMed]
9. Wang, L.; Wang, J.; Wang, Z.; Feng, J.; Li, S.; Yan, W. Synthesis of Ce-doped magnetic biochar for effective Sb(V) removal: Performance and mechanism. *Powder Technol.* **2019**, *345*, 501–508. [CrossRef]
10. Jia, X.; Zhou, J.; Liu, J.; Liu, P.; Yu, L.; Wen, B.; Feng, Y. The antimony sorption and transport mechanisms in removal experiment by Mn-coated biochar. *Sci. Total Environ.* **2020**, *724*, 138158. [CrossRef]
11. Dai, Y.; Zhang, N.; Xing, C.; Cui, Q.; Sun, Q. The adsorption, regeneration and engineering applications of biochar for removal organic pollutants: A review. *Chemosphere* **2019**, *223*, 12–27. [CrossRef]
12. Inyang, M.I.; Gao, B.; Yao, Y.; Xue, Y.; Zimmerman, A.; Mosa, A.; Pullammanappallil, P.; Ok, Y.S.; Cao, X. A review of biochar as a low-cost adsorbent for aqueous heavy metal removal. *Crit. Rev. Environ. Sci. Technol.* **2016**, *46*, 406–433. [CrossRef]
13. Kılıç, M.; Kırbıyık, Ç.; Çepeliogullar, Ö.; Pütün, A.E. Adsorption of heavy metal ions from aqueous solutions by bio-char, a by-product of pyrolysis. *Appl. Surf. Sci.* **2013**, *283*, 856–862. [CrossRef]
14. Qiu, B.; Tao, X.; Wang, H.; Li, W.; Ding, X.; Chu, H. Biochar as a low-cost adsorbent for aqueous heavy metal removal: A review. *J. Anal. Appl. Pyrolysis* **2021**, *155*, 105081. [CrossRef]
15. Han, L.; Sun, H.; Ro, K.; Sun, K.; Libra, J.; Xing, B. Removal of antimony (III) and cadmium (II) from aqueous solution using animal manure-derived hydrochars and pyrochars. *Bioresour. Technol.* **2017**, *234*, 77–85. [CrossRef] [PubMed]
16. Deng, J.; Li, X.; Wei, X.; Liu, Y.; Liang, J.; Shao, Y.; Huang, W.; Cheng, X. Different adsorption behaviors and mechanisms of a novel amino-functionalized hydrothermal biochar for hexavalent chromium and pentavalent antimony. *Bioresour. Technol.* **2020**, *310*, 123438. [CrossRef] [PubMed]
17. Lyonga, F.N.; Hong, S.-H.; Cho, E.-J.; Kang, J.-K.; Lee, C.-G.; Park, S.-J. As(III) adsorption onto Fe-impregnated food waste biochar: Experimental investigation, modeling, and optimization using response surface methodology. *Environ. Geochem. Health* **2021**, *43*, 3303–3321. [CrossRef] [PubMed]
18. Leuz, A.-K.; Mönch, H.; Johnson, C.A. Sorption of Sb(III) and Sb(V) to Goethite: Influence on Sb(III) Oxidation and Mobilization. *Environ. Sci. Technol.* **2006**, *40*, 7277–7282. [CrossRef] [PubMed]
19. Lee, N.; Hong, S.-H.; Lee, C.-G.; Park, S.-J.; Lee, J. Conversion of cattle manure into functional material to remove selenate from wastewater. *Chemosphere* **2021**, *278*, 130398. [CrossRef]
20. Qian, X.; Lee, S.; Chandrasekaran, R.; Yang, Y.; Caballes, M.; Alamu, O.; Chen, G. Electricity Evaluation and Emission Characteristics of Poultry Litter Co-Combustion Process. *Appl. Sci.* **2019**, *9*, 4116. [CrossRef]

21. Qian, X.; Yang, Y.; Lee, S.W. Design and Evaluation of the Lab-Scale Shell and Tube Heat Exchanger (STHE) for Poultry Litter to Energy Production. *Processes* **2020**, *8*, 500. [[CrossRef](#)]
22. Xin, Y.; Cao, H.; Yuan, Q.; Wang, D. Two-step gasification of cattle manure for hydrogen-rich gas production: Effect of biochar preparation temperature and gasification temperature. *Waste Manag.* **2017**, *68*, 618–625. [[CrossRef](#)]
23. Lee, J.; Sarmah, A.K.; Kwon, E.E. Chapter 1—Production and Formation of Biochar. In *Biochar from Biomass and Waste*; Ok, Y.S., Tsang, D.C.W., Bolan, N., Novak, J.M., Eds.; Elsevier: Amsterdam, The Netherlands, 2019; pp. 3–18. [[CrossRef](#)]
24. Tseng, R.-L.; Wu, P.-H.; Wu, F.-C.; Juang, R.-S. A convenient method to determine kinetic parameters of adsorption processes by nonlinear regression of pseudo-nth-order equation. *Chem. Eng. J.* **2014**, *237*, 153–161. [[CrossRef](#)]
25. Alberti, G.; Amendola, V.; Pesavento, M.; Biesuz, R. Beyond the synthesis of novel solid phases: Review on modelling of sorption phenomena. *Co-Ord. Chem. Rev.* **2012**, *256*, 28–45. [[CrossRef](#)]
26. Coates, J. *Encyclopedia of Analytical Chemistry*; Meyers, R.A., Ed.; John Wiley & Sons Ltd.: Chichester, UK, 2000; pp. 10815–10837.
27. Vithanage, M.; Rajapaksha, A.U.; Dou, X.; Bolan, N.; Yang, J.E.; Ok, Y.S. Surface complexation modeling and spectroscopic evidence of antimony adsorption on iron-oxide-rich red earth soils. *J. Colloid Interface Sci.* **2013**, *406*, 217–224. [[CrossRef](#)] [[PubMed](#)]
28. McComb, K.A.; Craw, D.; McQuillan, A.J. ATR-IR Spectroscopic Study of Antimonate Adsorption to Iron Oxide. *Langmuir* **2007**, *23*, 12125–12130. [[CrossRef](#)] [[PubMed](#)]
29. Lee, J.-I.; Hong, S.-H.; Lee, C.-G.; Park, S.-J. Experimental and model study for fluoride removal by thermally activated sepiolite. *Chemosphere* **2020**, *241*, 125094. [[CrossRef](#)] [[PubMed](#)]
30. Ho, Y. Review of second-order models for adsorption systems. *J. Hazard. Mater.* **2006**, *136*, 681–689. [[CrossRef](#)]
31. Edzwald, J.; American Water Works Association. *Water Quality & Treatment: A Handbook on Drinking Water*; McGraw-Hill Education: Denver, CO, USA, 2011.
32. Guo, X.; Wu, Z.; He, M.; Meng, X.; Jin, X.; Qiu, N.; Zhang, J. Adsorption of antimony onto iron oxyhydroxides: Adsorption behavior and surface structure. *J. Hazard. Mater.* **2014**, *276*, 339–345. [[CrossRef](#)] [[PubMed](#)]
33. Qi, Z.; Joshi, T.P.; Liu, R.; Li, Y.; Liu, H.; Qu, J. Adsorption combined with superconducting high gradient magnetic separation technique used for removal of arsenic and antimony. *J. Hazard. Mater.* **2018**, *343*, 36–48. [[CrossRef](#)]
34. Li, D.; Hu, X.; Sun, Y.; Su, S.; Xia, A.; Ge, H. Goethite (α -FeOOH) nanopowders synthesized via a surfactant-assisted hydrothermal method: Morphology, magnetic properties and conversion to rice-like α -Fe₂O₃ after annealing. *RSC Adv.* **2015**, *5*, 27091–27096. [[CrossRef](#)]
35. Lee, J.-I.; Kang, J.-K.; Hong, S.-H.; Lee, C.-G.; Jeong, S.; Park, S.-J. Thermally treated Mytilus coruscus shells for fluoride removal and their adsorption mechanism. *Chemosphere* **2021**, *263*, 128328. [[CrossRef](#)]
36. Mbamba, C.K. Dynamic Modelling of Minerals Precipitation in Wastewater Treatment. Ph.D. Thesis, University of Queensland Library, Brisbane, QLD, Australia, 2016.
37. He, Z.; Liu, R.; Liu, H.; Qu, J. Adsorption of Sb(III) and Sb(V) on Freshly Prepared Ferric Hydroxide (FeOxHy). *Environ. Eng. Sci.* **2015**, *32*, 95–102. [[CrossRef](#)]
38. Kang, J.-K.; Seo, E.-J.; Lee, C.-G.; Park, S.-J. Fe-loaded biochar obtained from food waste for enhanced phosphate adsorption and its adsorption mechanism study via spectroscopic and experimental approach. *J. Environ. Chem. Eng.* **2021**, *9*, 105751. [[CrossRef](#)]